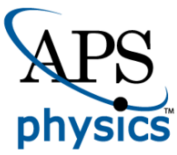

Topologically Protected Complete Polarization Conversion

Yu Guo, Meng Xiao, and Shanhui Fan

Phys. Rev. Lett. **119**, 167401 — Published 18 October 2017

DOI: 10.1103/PhysRevLett.119.167401

Topologically protected complete polarization conversion

Yu Guo, Meng Xiao, Shanhui Fan*
Department of Electrical Engineering, Ginzton Laboratory, Stanford University, Stanford, California 94305, USA

We consider the process of conversion between linear polarizations as light is reflected from a photonic crystal slab. We observe that, over a wide range of frequencies, complete polarization conversion can be found at isolated wavevectors. Moreover, such an effect is topological: the complex reflection coefficients have a non-zero winding number in the wavevector space. We also show that bound states in continuum in this system have their wavevectors lying on the critical coupling curve that defines the condition for complete polarization conversion. Our work points to the use of topological photonics concepts for the control of polarization, and suggests the exploration of topological properties of scattering matrices as a route towards creating robust optical devices.

There are now significant interests in exploiting topological properties in a wide variety of physical systems. In general, topologically-nontrivial systems are characterized by topological invariants that take integer values. Since an integer cannot be continuously changed, physical quantities associated with the invariant can be robust against small perturbations. Applying topological concepts to optics has led to the development of topological photonics [1, 2]. At present, most efforts in this field have been devoted to the study of topological invariants such as the Chern number in the photonic band structures of bulk photonic crystal and metamaterial structures, where a nonzero Chern number implies the existence of topologically-nontrivial edge states [3–13]. But there are also emerging interests in extending topological photonics concepts beyond band structure analysis. For example, it has been recently noted that bound states in continuum [14, 15], i.e., resonances with infinite quality factors, are topological in nature [16].

In this Letter we seek to extend topological concepts to the analysis of scattering matrices. The response of any linear optical devices is characterized by its scattering matrix, the elements of which are mode-to-mode transmission and reflection coefficients. Here as an illustration we consider the process of conversion between linear polarizations for light reflected from a photonic crystal slab. Using both numerical studies and analytic theory, we show that a photonic crystal slab can provide complete polarization conversion in a reflection process, which is a topological effect since the complex reflection coefficients have a nonzero winding number in the wavevector space. Consequently, complete polarization conversion can be observed over a wide range of frequencies. We also identify an interesting connection between complete polarization conversion and bound states in continuum [14–16]: these bound states always lie on the critical coupling curve that defines the condition for complete polarization conversion.

Polarization is one of the most fundamental properties of light. There have been significant recent efforts in using various photonic structures to achieve polarization conversion [17–27]. Our result points to the use of topological photonics concepts to achieve polarization control. More generally, our work should motivate systematic studies of topological properties of scattering matrices as a route towards creating robust optical devices.

Our structure consists of a photonic crystal slab patterned with a square array of air holes introduced into the dielectric slab and a mirror underneath, as illustrated in Fig. 1(a). The periodicity of the crystal is chosen such that within the wavelength range of interest only zeroth order diffraction can occur in free space upon light incident from different angles. As a result, our structure is characterized by the 2×2 reflection matrix,

$$R = \begin{pmatrix} R_{ss} & R_{sp} \\ R_{ps} & R_{pp} \end{pmatrix}. \tag{1}$$

Here $R_{\sigma\mu}$ denotes the reflection coefficient of μ-polarized incident wave reflected into σ-polarized wave, where $\sigma, \mu \in \{s, p\}$. The polarization is defined with respect to propagation direction indicated by a unit vector $\hat{k}$, that is, $\hat{s} = \hat{z} \times \hat{k}$, $\hat{p} = \hat{s} \times \hat{k}$, where $\hat{z}$ is the unit vector perpendicular to the slab.

We consider the lossless case first, where R is unitary. As a result, complete polarization conversion, as described by $|R_{sp}| = |R_{ps}| = 1$, is equivalent to $R_{ss} = 0$. We focus on R_{ss} since the zero of a complex function may be topological.

We consider a structure with $\epsilon = 12$, $h = 0.3a$, $r = 0.3a$, where ϵ is the dielectric constant of the slab, a is the periodicity, h is the thickness of the slab, and r is the radius of the air hole. In Fig. 1(b), we plot the spectrum of R_{ss} computed using the rigorous coupled wave analysis [28] for incident waves at two different parallel wavevectors $k_\parallel = (k_x, k_y)$. The blue curve shows $|R_{ss}|^2$ at $k_{\parallel,1} = (0.0240, 0.0522)2\pi/a$, the red curve shows $|R_{ss}|^2$ at $k_{\parallel,2} = (0.0345, 0.0717)2\pi/a$. We observe $R_{ss} = 0$ at $\omega_{0,1} = 0.388 \times 2\pi c/a$ and $\omega_{0,2} = 0.385 \times 2\pi c/a$, respectively, indicating complete polarization conversion. In Fig. 1(c) and (d), we show the amplitudes of reflection coefficients R_{ss} as a function of the parallel wavevector $k_\parallel$ at $\omega_{0,1}$ and $\omega_{0,2}$, respectively. At both frequencies, we observe $R_{ss} = 0$ at two isolated wavevectors related by the

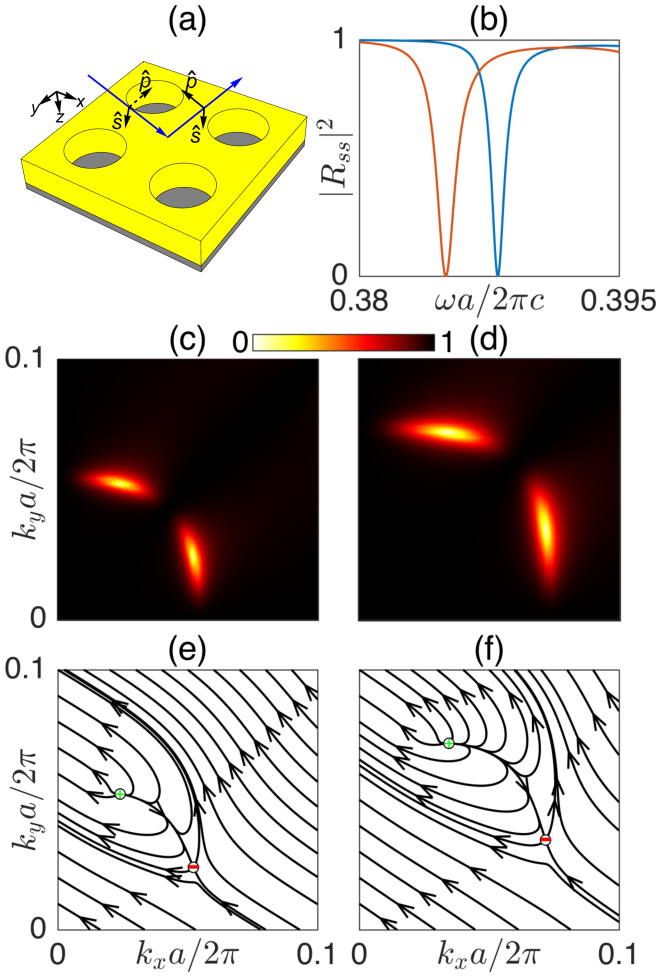

FIG. 1. (a) Schematic of the structure. A dielectric photonic crystal is sitting on top of a perfect mirror. We denote the dielectric constant of the slab by ϵ, the periodicity by a, the thickness of the slab by h, the radius of the air hole by r. For the other subplots, the parameters are $\epsilon = 12, h = 0.3a, r = 0.3a$. (b) Blue curve: reflection spectrum at $k_{\parallel,1} = (0.0240,\ 0.0522)2\pi/a$. Red curve: reflection spectrum at $k_{\parallel,2} = (0.0345,\ 0.0717)2\pi/a$. The complete conversion where $R_{ss} = 0$ occurs at $\omega_{0,1} = 0.388 \times 2\pi c/a$ and $\omega_{0,2} = 0.385 \times 2\pi c/a$, respectively. (c, d) $|R_{ss}|$ at the frequency (c) $\omega_{0,1}$, (d) $\omega_{0,2}$. (e, f) Direction flow of vector field $(\mathrm{Re}(R_{ss}), \mathrm{Im}(R_{ss}))$ at the frequency (e) $\omega_{0,1}$, (f) $\omega_{0,2}$.

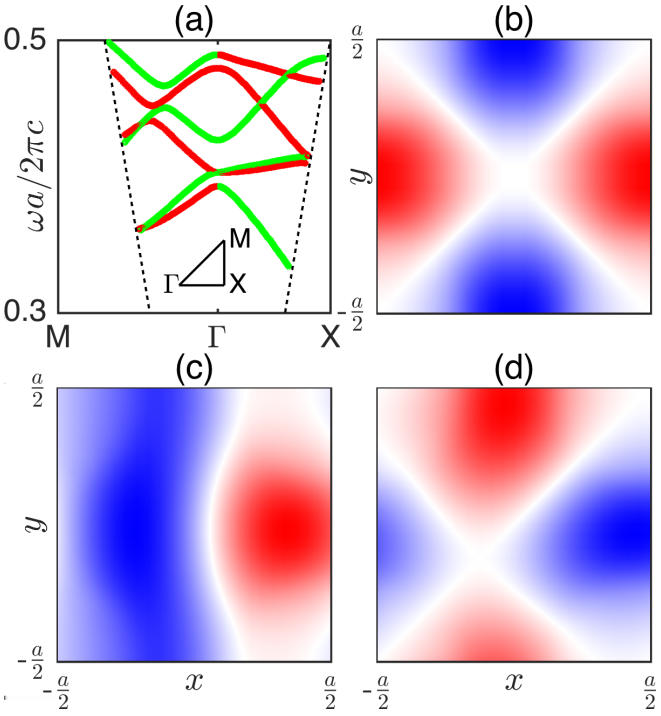

FIG. 2. (a) Band diagram of the structure in Fig. 1(a) with $\epsilon = 12$, $h = 0.3a$, $r = 0.3a$. The dash lines denote the light cone. (b, c, d) Electric field ($\mathrm{Re}(E_z)$) distribution of the lowest order guided resonance at the interface between photonic crystal slab and mirror at (b) Γ point, (c) $(k_x,\ k_y) = (0.1,\ 0.0)2\pi/a$ on ΓX, (d) $(k_x,\ k_y) = (0.1,\ 0.1)2\pi/a$ on ΓM.

point group symmetry of the lattice. Numerically, when varying the incident frequency from $\omega = 0.40 \times 2\pi c/a$ to $\omega = 0.35 \times 2\pi c/a$, we observe the wavevectors at which $R_{ss} = 0$ shift from the Γ point towards the light cone. The effect of complete polarization conversion is therefore robust with respect to frequency variation.

We now numerically demonstrate that the zeros in R_{ss} have non-trivial topological properties. Since R_{ss} is complex, we consider a vector field of $(\mathrm{Re}(R_{ss}), \mathrm{Im}(R_{ss}))$, and compute the winding number of the vector field along a closed path in the (k_x, k_y) space around the wavevectors where $R_{ss} = 0$. To visualize the winding number, in Fig. 1(e) and (f), we plot the direction flow of the $(\mathrm{Re}(R_{ss}), \mathrm{Im}(R_{ss}))$ vector field at $\omega_{0,1}$ and $\omega_{0,2}$, respectively. We observe a saddle point that has a winding number of -1, at $k_{\parallel,1}$, $k_{\parallel,2}$ in Fig. 1(e) and (f), respectively. We also observe a source point that has a winding number of $+1$ in the upper triangular region with $k_y > k_x$. The source point is connected with the saddle point by the mirror operation with respect to the $x = y$ plane. Such a mirror operation flips the sign of the topological charge. The nonzero winding numbers associated with the zeros of R_{ss} indicate that the effect of complete polarization conversion is topological in nature.

Motivated by the numerical observation above, we now present an analytic theory that provides insight into the physical mechanism through which the non-trivial topological feature is generated. The results shown in Fig. 1 occur when the incident wave excites guided resonances [29]. From the temporal coupled mode theory [30, 31], the reflection matrix R in the vicinity of a non-degenerate guided resonance can be expressed as [32]

$$R = -\sigma_z (I - \frac{dd^\dagger}{i(\omega_0 - \omega) + \gamma}) C, \tag{2}$$

where $C = diag(C_{ss}, C_{pp})$ is the background reflection matrix, $\sigma_z = diag(1, -1)$, I is the 2×2 identity matrix,

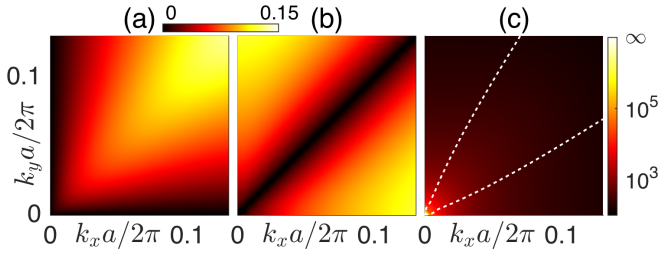

FIG. 3. The parameters are $\epsilon = 12$, $h = 0.3a$, $r = 0.3a$, which are same to that in Fig. 1 and Fig. 2. (a) Amplitude of coupling constant to s-polarized waves of the lowest band, denoted by $|d^s|$. $|d^s|$ is zero along ΓX. (b) Amplitude of coupling constant to p-polarized waves of the lowest band, denoted by $|d^p|$. $|d^p|$ is zero along ΓM. (c) The background shows quality factor of the lowest order resonances in a logarithmic scale. The dashed curve denotes the critical coupling curve on which $|d^s| = |d^p|$.

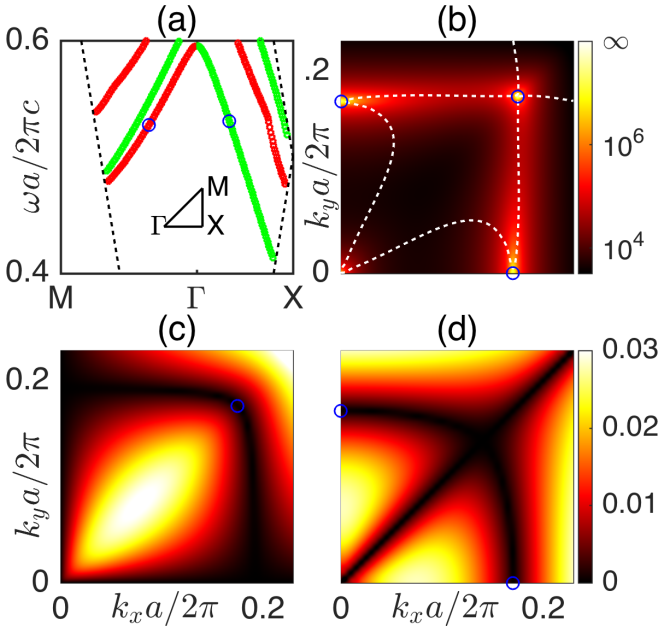

FIG. 4. The parameters here are $\epsilon = 4$, $h = 0.9a$, $r = 0.4a$. (a) Band diagram of the structure. The dash lines enclose the region where only zeroth order diffraction can occur. The two blue circles indicate guided resonances with infinite quality factor. (b) The background shows quality factor of the lowest order resonances in a logarithmic scale. The dashed curve denotes the critical coupling curve on which $|d^s| = |d^p|$. The blue circles indicate the wavevectors of the non-symmetry-protected bound states in continuum where $|d^s| = |d^p| = 0$. (c) Amplitudes of coupling constants to s-polarized waves of the lowest band, denoted by $|d^s|$. The blue circle indicates the wavevector on ΓM for which $|d^s| = 0$. (d) Amplitude of coupling constant to p-polarized waves of the lowest band, denoted by $|d^p|$. The blue circle indicates the wavevector on ΓX for which $|d^p| = 0$.

$d = (d^s, d^p)^T$, in which d^s, d^p are the coupling constant of the resonance to s- and p-polarized waves, respectively, γ is the radiation loss rate of the resonance, and ω_0 is the resonant frequency. At $\omega = \omega_0$, if $|d^s| = |d^p| \neq 0$, then $R_{ss} = 0$, which implies complete polarization conversion. Since in our scenario, the resonance can only couple to two linear polarization radiation channels, the condition of $|d^s| = |d^p|$ is equivalent to the condition of Q-matching to achieve perfect transmission in resonant filter, or the condition of critical coupling to achieve complete absorption in a resonant absorber. Below, we refer to the condition $|d^s| = |d^p|$ as the critical coupling condition.

The guided resonances form photonic bands. On each band, to achieve complete polarization conversion, we need to find the *critical coupling curve* on which $|d^s| = |d^p|$. We demonstrate that the existence of the critical coupling curve is guaranteed by the C_{4v} symmetry of the structure. We plot the band diagram in Fig. 2(a). The color in the band diagram reflects the parity of the modes, red for odd modes, green for even modes, where the corresponding mirror plane is $y = 0$ for wavevectors along ΓX and $x = y$ for wavevectors along ΓM. For the lowest band, the eigenmode at the Γ point has a one-dimensional irreducible representation B_1 [33], where the eigenvalues of operations C_4 (rotation by $\pi/2$ around the z-axis), σ_v (mirror with respect to $y = 0$) and σ_d (mirror with respect to $x = y$) are -1, 1, -1, respectively, as seen in Fig. 2(b). From the compatibility relations [33], wavevectors along ΓX belong to the A representation of the C_{1h} point group, where the eigenmode is even with respect to the mirror plane $y = 0$ (Fig. 2(c)), and wavevectors along ΓM belong to the B representation of the C_{1h} point group, where the eigenmode is odd with respect to the mirror plane $x = y$ (Fig. 2(d)).

Clearly, odd modes can only couple to s-polarized waves and even modes can only couple to p-polarized waves. For the lowest band shown in Fig. 2, along ΓX, the coupling rate to s-polarized wave d^s is zero, whereas along ΓM, the coupling rate to p-polarized wave d^p is zero. Thus for a point Δ on ΓX, the coupling constants of the lowest band satisfy $|d^p(\Delta)| \geq |d^s(\Delta)| = 0$, whereas for a point Σ on ΓM, $|d^s(\Sigma)| \geq |d^p(\Sigma)| = 0$. On a line segment connecting these two points Δ and Σ inside the reduced Brillouin zone, there must be at least one point where $|d^s| = |d^p|$. At this point we have complete polarization conversion unless $|d^s| = |d^p| = 0$.

To verify our theory, we compute the coupling constants of the lowest band [34], as shown in Fig. 3. d^s and d^p are indeed zero along ΓX and ΓM, respectively, as argued above and shown in Fig. 3(a) and (b). And we indeed observe the critical coupling curve in k-space shown as the dashed curve in Fig. 3(c). Also, with the coupled mode theory (Eq. (2)) and the numerical results of the coupling constants, we have confirmed that at each frequency within the lowest band the zeros of R_{ss} on the lower (upper) critical coupling curve in Fig. 3(c) indeed

have a winding number of -1 $(+1)$, consistent with the direct numerical calculations presented above [35].

We note an interesting connection between complete polarization conversion, and bound states in the continuum as discussed in Refs. [14] and [16]. The Γ point lies on the critical coupling curve as shown by the dashed curve in Fig. 3(c). For this particular band, at the Γ point the resonance is singly degenerate and cannot couple to external radiation modes, and hence has a diverging quality factor shown in Fig. 3(c). Therefore, this resonance at the Γ point is a bound state in continuum. In general, the bound state in continuum always lies on the critical coupling curve, since at a bound state both d^s and d^p vanishes, we have $|d^s| = |d^p|$. Of course, exactly at a bound state there is no polarization conversion. But in the immediate vicinity of a bound state there is always a wavevector where complete polarization conversion occurs. The frequency bandwidth over which significant polarization conversion occurs vanishes as one approaches a bound state.

In Fig. 3(c), the bound state at the Γ point is protected by symmetry. On the other hand, there is a recent discovery of a new type of bound states in continuum that is not protected by symmetry [14, 16]. The argument presented above applies to both types of bound states. Thus, we expect that the non-symmetry-protected bound state in continuum should appear on the critical coupling curve as well. As an illustration, we consider a photonic crystal slab structure with the parameters $\epsilon = 4, h = 0.9a, r = 0.4a$. Fig. 4(a) shows the band diagram for this structure. Examining the quality factor of the lowest order guided resonances in the wavevector space (Fig. 4(b)), we find two distinct non-symmetry-protected bound states with infinite quality factors indicated by the blue circles, one on ΓX, the other on ΓM, in addition to the symmetry-protected bound state at the Γ point. Fig. 4(c) and (d) show the amplitudes of d^s and d^p of the lowest band, respectively. In addition to being zero due to mirror symmetry, both d^s and d^p are zero at the wavevector where the non-symmetry-protected bound states in continuum occur, as indicated by blue circles. In Fig. 4(b), we also show the critical coupling curve on which $|d^s| = |d^p|$, and indeed non-symmetry-protected bound states in continuum lie on this curve. Our results indicate an intriguing connection between the two topological photonics effects of complete polarization conversion, and bound states in continuum.

Our structure also exhibits unusual effects on circularly polarized waves. Denote the left and right handed circularly polarized waves by $|L\rangle$ and $|R\rangle$, which can be represented by $(1, \mp i)^T$ in the linear polarized $\hat{s}$, $\hat{p}$ basis. Ordinary mirrors, where the reflection matrix $R = [-1, 0; 0, 1]$, reverses the handedness of incident circularly polarized wave, e.g., $R|L\rangle = -|R\rangle$ and $R|R\rangle = -|L\rangle$. For our structure, due to reciprocity and inversion symmetry, we find that $R_{ps}(k) = -R_{sp}(k)$, which fixes the relative phase of $R_{ps}(k)$ and $R_{sp}(k)$. Without loss of generality, we can write the reflection matrix R at complete polarization conversion as $[0, 1; -1, 0]$. Upon reflection, one finds $R|L\rangle = -i|L\rangle$ and $R|R\rangle = i|R\rangle$. Therefore, in contrast to regular mirrors which flips handedness upon reflection, our structure can completely reflect the incident circularly polarized wave while preserving its handedness.

The robustness of the complete polarization conversion effect comes from the fact that the eigenmodes on ΓX and ΓM posses opposite parities with respect to their corresponding mirror plane. Though in this work we focus on the lowest band, it is clear that any bands where the Γ point belong to the B_1 or B_2 representation [33] of the C_{4v} group should be able to achieve complete polarization conversion as well. For a given structure, complete polarization conversion can occur over a broad range of frequencies. At each of these frequencies, there exist angles at which complete polarization conversion occurs. At a fixed incident frequency, the operating angular bandwidth is inversely proportional to the quality factor of the guided resonance, which is tunable by varying the dielectric constant or geometrical parameters [36–38].

As a final remark, we briefly comment on the effects of loss, with a more detailed discussion provided in the Supplementary Material [39]. We gradually increase the loss of the dielectric slab and examine how it affects the zeros of R_{ss}. For illustration, we choose $h = 0.3a$, $r = 0.3a$, fix the real part of ϵ to be 12, and vary the imaginary part of ϵ. As we increase the imaginary part of ϵ from zero, we observe that the two opposite charges of R_{ss} move towards each other, and annihilate on the diagonal line $k_x = k_y$ at $\mathrm{Im}(\epsilon) \approx 0.04$ [39]. The efficiency of polarization conversion, i.e. $|R_{ps}|^2$, generally decreases as the loss increases. Nevertheless, in the wavevector regions where the radiation loss rate of the guided resonance dominates the material loss rate, one can observe near perfect polarization conversion even in the presence of realistic loss. On the other hand, the effect of $R_{ss} = 0$ is topological, and hence there is always a wavevector at which R_{ss} remains exactly zero as modest amount of loss is added in the system. Our results thus point to the manifestation of an interesting effect that is topologically protected against loss.

To summarize, we identify a non-trivial topological effect in the reflection matrix of a simple photonic crystal slab, which leads to a capability for controlling the polarization of light. In this system, the non-trivial topology arises since the underlying map is from a two-dimensional momentum space to a complex field. We expect a richer set of topological phenomena as we consider maps from higher dimensional space to other aspects of the scattering matrix that defines optical devices. Our work should point to a fruitful avenue where we use the concepts of topology to design optical devices.

Y.G. is grateful to Yang Zhou, Yu (Jerry) Shi, Qian

Lin, Dr. Alexander Cerjan and Dr. Chia Wei Hsu for helpful discussions. The authors acknowledge the support of the National Science Foundation (Grant No. CBET-1641069), and the Air Force Office of Scientific Research (FA9550-16-1-0010, FA9550-17-1-0002).

* shanhui@stanford.edu

[1] L. Lu, J. D. Joannopoulos, and M. Soljačić, Nat. Photonics **8**, 821 (2014).
[2] L. Lu, J. D. Joannopoulos, and M. Soljačić, Nat. Phys. **12**, 626 (2016).
[3] F. D. M. Haldane and S. Raghu, Phys. Rev. Lett. **100**, 013904 (2008).
[4] Z. Wang, Y. D. Chong, J. D. Joannopoulos, and M. Soljačić, Phys. Rev. Lett. **100**, 013905 (2008).
[5] Z. Wang, Y. Chong, J. D. Joannopoulos, and M. Soljačić, Nature **461**, 772 (2009).
[6] K. Fang, Z. Yu, and S. Fan, Nat. Photonics **6**, 782 (2012).
[7] M. C. Rechtsman, J. M. Zeuner, Y. Plotnik, Y. Lumer, D. Podolsky, F. Dreisow, S. Nolte, M. Segev, and A. Szameit, Nature **496**, 196 (2013).
[8] M. Hafezi, S. Mittal, J. Fan, A. Migdall, and J. M. Taylor, Nat. Photonics **7**, 1001 (2013).
[9] W.-J. Chen, S.-J. Jiang, X.-D. Chen, B. Zhu, L. Zhou, J.-W. Dong, and C. T. Chan, Nat. Commun. **5**, 5782 (2014).
[10] L.-H. Wu and X. Hu, Phys. Rev. Lett. **114**, 223901 (2015).
[11] X. Cheng, C. Jouvaud, X. Ni, S. H. Mousavi, A. Z. Genack, and A. B. Khanikaev, Nat. Mater. **15**, 542 (2016).
[12] Y. Poo, R.-x. Wu, Z. Lin, Y. Yang, and C. T. Chan, Phys. Rev. Lett. **106**, 093903 (2011).
[13] C. He, X.-C. Sun, X.-P. Liu, M.-H. Lu, Y. Chen, L. Feng, and Y.-F. Chen, PNAS **113**, 4924 (2016).
[14] C. W. Hsu, B. Zhen, J. Lee, S.-L. Chua, S. G. Johnson, J. D. Joannopoulos, and M. Soljačić, Nature **499**, 188 (2013).
[15] C. W. Hsu, B. Zhen, A. D. Stone, J. D. Joannopoulos, and M. Soljačić, Nat. Rev. Mater. **1**, 16048 (2016).
[16] B. Zhen, C. W. Hsu, L. Lu, A. D. Stone, and M. Soljačić, Phys. Rev. Lett. **113**, 257401 (2014).
[17] S. J. Elston, G. P. Bryan-Brown, and J. R. Sambles, Phys. Rev. B **44**, 6393 (1991).
[18] J. Hao, Y. Yuan, L. Ran, T. Jiang, J. A. Kong, C. T. Chan, and L. Zhou, Phys. Rev. Lett. **99**, 063908 (2007).
[19] J. Hao, Q. Ren, Z. An, X. Huang, Z. Chen, M. Qiu, and L. Zhou, Phys. Rev. A **80**, 023807 (2009).
[20] Y. Ye and S. He, Appl. Phys. Lett. **96**, 203501 (2010).
[21] C. Huang, Y. Feng, J. Zhao, Z. Wang, and T. Jiang, Phys. Rev. B **85**, 195131 (2012).
[22] N. K. Grady, J. E. Heyes, D. R. Chowdhury, Y. Zeng, M. T. Reiten, A. K. Azad, A. J. Taylor, D. A. R. Dalvit, and H.-T. Chen, Science **340**, 1304 (2013).
[23] H. L. Zhu, S. W. Cheung, K. L. Chung, and T. I. Yuk, IEEE Trans. Antennas Propag. **61**, 4615 (2013).
[24] L. Cong, W. Cao, X. Zhang, Z. Tian, J. Gu, R. Singh, J. Han, and W. Zhang, Appl. Phys. Lett. **103**, 171107 (2013).
[25] Y. Yang, W. Wang, P. Moitra, I. I. Kravchenko, D. P. Briggs, and J. Valentine, Nano Lett. **14**, 1394 (2014).
[26] F. Ding, Z. Wang, S. He, V. M. Shalaev, and A. V. Kildishev, ACS Nano **9**, 4111 (2015).
[27] H. Sun, C. Gu, X. Chen, Z. Li, L. Liu, and F. Martín, Journal of Applied Physics **121**, 174902 (2017).
[28] V. Liu and S. Fan, Computer Physics Communications **183**, 2233 (2012).
[29] S. Fan and J. D. Joannopoulos, Phys. Rev. B **65**, 235112 (2002).
[30] H. A. Haus, *Waves and Fields in Optoelectronics*, Vol. 464 (Prentice-Hall Englewood Cliffs, NJ, 1984).
[31] S. Fan, W. Suh, and J. D. Joannopoulos, J. Opt. Soc. Am. A **20**, 569 (2003).
[32] See Section I of Supplemental Material for a derivation of this equation.
[33] K. Sakoda, *Optical Properties of Photonic Crystals*, Vol. 80 (Springer, 2004).
[34] See Section II of Supplemental Material for a description on the numerical methods.
[35] See Section III of Supplemental Material for a first order perturbation theory around the zeros of R_{ss}.
[36] J. R. Piper and S. Fan, ACS Photonics **1**, 347 (2014).
[37] Y. Guo and S. Fan, Opt. Express **24**, 29896 (2016).
[38] See Section IV of Supplemental Material for a discussion on the angular dependence of polarization conversion efficiency.
[39] See Section V of Supplemental Material for a discussion on the effects of material loss.